

## Supporting information

### Three-dimensional layered double hydroxide membranes: fabrication technique, growth mechanism, and enhanced photocatalytic activity

Li Xue,<sup>a</sup> Zhipeng Lü,<sup>a</sup> Yingzhi Cheng,<sup>\*a</sup> Xiuyu Sun,<sup>a</sup> Hongtao Lin,<sup>a</sup> Xiaoling Xiao,<sup>b</sup>  
Xiangfeng Liu<sup>b</sup> and Shuping Zhuo<sup>\*a</sup>

<sup>a</sup> School of Chemistry and Chemical Engineering, Shandong University of Technology, Zibo 255049, China

<sup>b</sup> College of Materials Science and Opto-Electronic Technology, University of Chinese Academy of Sciences, Beijing 100049, China

\*Corresponding Author: chengyz@sdut.edu.cn, zhuosp\_academic@yahoo.com

#### Experimental Section

All reagents were analytical grade without further purification.

**AAO Preparation.** Pure aluminum sheets (99.995%, 0.2 mm in thickness, General Research Institute for Nonferrous Metals, Beijing) were rinsed with ethanol, 0.5 M NaOH solution, and deionized water in sequence. After electropolished in chromic acid solution, the aluminum sheets were anodized at 160 V for 32 h in a phosphoric acid solution. The barrier layer of anodic aluminum oxide (AAO) was removed in a 0.5 M phosphoric acid solution to prepare self-supporting through-hole AAO templates.

**Sample Preparation.** A precipitant-free in situ growth technique was used to fabricate the three-dimensional ZnAl-LDH/AAO and NiAl-LDH/AAO membranes. Typically, AAO templates (2 cm in diameter) were placed vertically in beakers containing Zn(NO<sub>3</sub>)<sub>2</sub>·6H<sub>2</sub>O or Ni(NO<sub>3</sub>)<sub>2</sub>·6H<sub>2</sub>O aqueous solutions. The beakers were then heated in a water bath at 80 °C for different hours. The resulting membranes were rinsed with deionized water and dried under ambient conditions over night. If necessary, the pH of given solutions were adjusted by nitric acid or ammonia solution. The CoAl-LDH/AAO and NiAl-LDH/AAO membranes were also fabricated in

water or ethanol solvent using the in situ growth method. The as-prepared samples were denoted as  $M_{x,t,y}(pH_z)$  (M:  $Zn^{2+}$ ,  $Ni^{2+}$  or  $Co^{2+}$ ; x: concentration of  $Zn^{2+}$ ,  $Ni^{2+}$  or  $Co^{2+}$  in reaction solutions; y: reaction time, z: the pH of reaction solution which pH had been adjusted from natural value). WAAO was prepared by soaking an AAO template in deionized water at 80 °C for 12 h. No precipitate was observed in reaction solutions of all samples during the whole processes. For comparison of photocatalytic activity, the NiAl-LDH/Al film catalyst was prepared by sinking a aluminum sheet (2 cm × 3 cm) in a 0.1 M  $Ni^{2+}$  solution with initial pH 2.0 at 80 °C for 24 h.<sup>1</sup>

**Characterization.** The crystallinity, morphology, composition, and surface nature of samples were investigated by conventional examination techniques. X-Ray diffraction (XRD) patterns were recorded on a Bruker D8 Advance X-ray diffractometer (Cu  $K\alpha$  radiation,  $\lambda = 1.5406 \text{ \AA}$ ) at 35 kV, 30 mA, with a scan step of  $0.02^\circ$  and a  $2\theta$  angle ranging from  $5^\circ$  to  $70^\circ$ . Fourier transform infrared (FT-IR) spectra of milled samples were recorded in KBr pellets on a Nicolet 5700 Fourier transformation infrared spectroscope (Thermo Electron Co., USA) from 4000 to  $400 \text{ cm}^{-1}$ , with a resolution of  $2 \text{ cm}^{-1}$ . Field emission scanning electron microscope (SEM) was carried out on a FEI Sirion 200 instrument with an energy dispersive X-ray spectrometer (EDX) unit (INCA Oxford). The accelerating voltage applied was 10 kV. All samples were sputtered with platinum. The regions analyzed by EDX were about  $10 \mu\text{m} \times 10 \mu\text{m}$  in the middle of cross section and on the outer surface of samples. X-ray photoelectron spectroscopy (XPS) spectra were performed on a Thermo SCIENTIFIC ESCALAB 250Xi X-ray photoelectron spectrometer using Al  $K\alpha$  radiation (1486.6 eV) with constant pass energy of 20 eV. All spectra were referenced to the C 1s signal at 284.8 eV.

**Photocatalytic test.** The photocatalytic activities of samples were investigated by the photocatalytic degradation of methyl orange (MO) in aqueous solution. A 100 mL of  $30 \text{ mg}\cdot\text{L}^{-1}$  MO solution was placed in a photocatalytic reactor, and a sheet of catalyst was suspended in the MO solution. After stirred for 30 min under dark to evaluate the adsorption of MO, the solution was irradiated immediately with ultraviolet light from a high-pressure mercury lamp (125 W, GGZ-125, Shanghai Yaming Fiya Lighting

Appliance Co., Ltd.,  $\lambda_{\max} = 365 \text{ nm}$ , average radiation intensity,  $7 \text{ mW/cm}^3$ ) hanging above the reactor. The temperature of the MO solution was controlled at room temperature by circulating water, and the concentration of MO was analyzed by colorimetry using a UV-1801 UV/VIS spectrophotometer (Beijing Beifen-Ruili Analytical Instrument (Group) Co., Ltd.) at intervals of 10 min. A blank reaction was also carried out without any catalyst.

Charge carrier trapping experiments have been studied using  $\text{N}_2$ , isopropanol (IPA), and triethanolamine (TEOA) as scavengers for  $\cdot\text{O}_2^-$ ,  $\cdot\text{OH}$ , and  $\text{h}^+$ , respectively, to elucidate the dominant reactive species involved in the degradation process. The stability tests are performed using 70 mL,  $20 \text{ mg}\cdot\text{L}^{-1}$  colorless 2,4-dichlorophenol (2,4-DCP) solutions instead of MO solutions. After the reaction, the photocatalyst was washed, and then used for the next cycle.

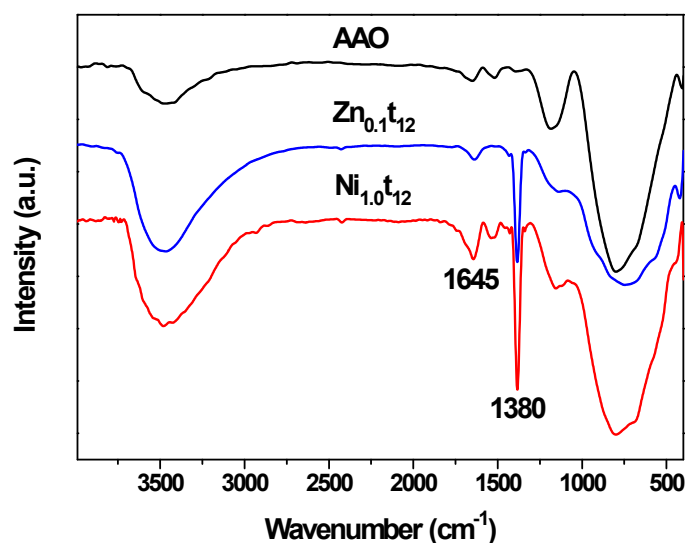


Fig. S1 FT-IR spectra of AAO,  $\text{Zn}_{0.1}\text{t}_{12}$ , and  $\text{Ni}_{1.0}\text{t}_{12}$ .

The broad and intense bands centered around  $3476 \text{ cm}^{-1}$  of  $\text{Zn}_{0.1}\text{t}_{12}$  and  $\text{Ni}_{1.0}\text{t}_{12}$  are due to the OH stretching mode of layer hydroxyl groups and interlayer water molecules in LDHs.<sup>1-3</sup> As for AAO template, this band is due to the hydroxyl groups on surface. The weak peak centered at  $1641 \text{ cm}^{-1}$  is associated with the bending mode of water.<sup>2-4</sup> The sharp peaks at  $1384 \text{ cm}^{-1}$  for  $\text{Zn}_{0.1}\text{t}_{12}$ , and  $\text{Ni}_{1.0}\text{t}_{12}$  are ascribable to the stretching mode of the nitrate anions, confirming the presence of  $\text{NO}_3^-$  anions in

ZnAl-LDH and NiAl-LDH.<sup>3,4</sup> According to the references,<sup>2,4</sup> the band in the range of 500–800  $\text{cm}^{-1}$  is mainly assigned to M–O–M bonds or translation modes of the hydroxyl groups influenced by  $\text{Al}^{3+}$ .

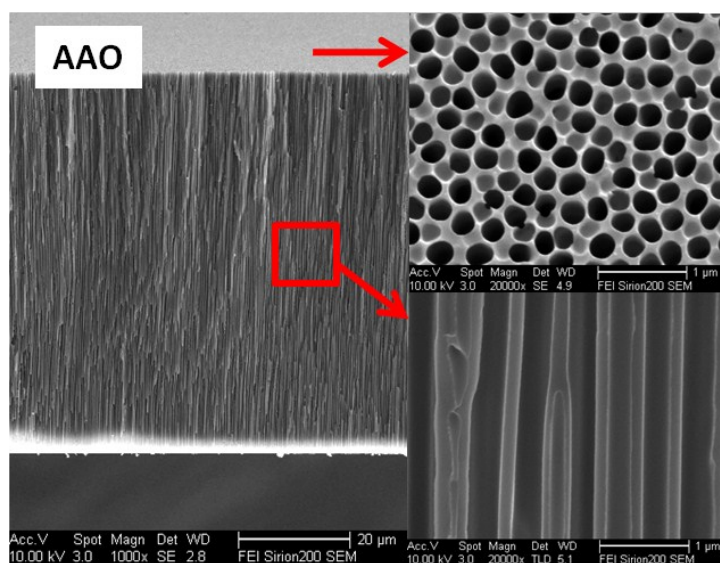


Fig. S2 SEM images of AAO template.

Fig. S2 shows the SEM images of top view and section view of as-prepared AAO template. The thickness of the AAO was about 70  $\mu\text{m}$  and the pore size was in the range of 270–310 nm.

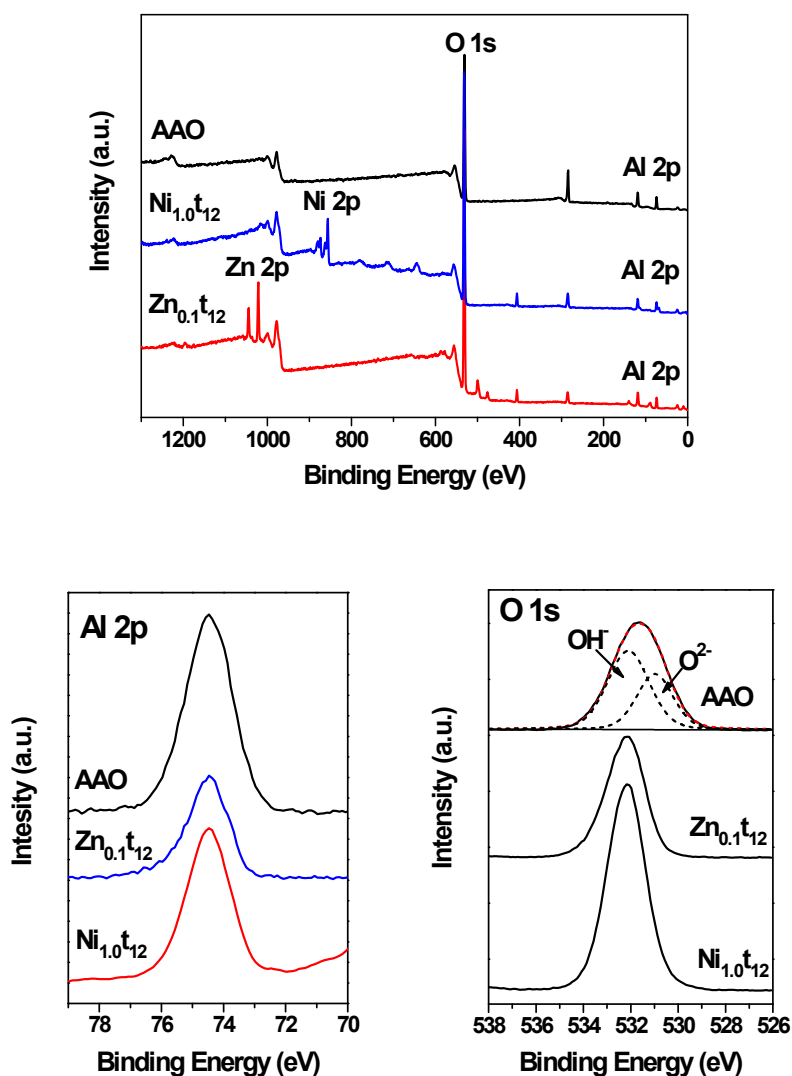


Fig. S3 XPS spectra of AAO template,  $\text{Zn}_{0.1}\text{t}_{12}$ , and  $\text{Ni}_{1.0}\text{t}_{12}$ .

The XPS results of full spectra, Al 2p and O 1s are given in Fig. S3. The binding energy (BE) values of Al 2p are approximately at 74.5 eV. As for O 1s, AAO template shows a wide peak containing two peaks at the BE of 531.0 eV and 532.0 eV, which are corresponded to the characteristic of O<sup>2-</sup> and OH<sup>-</sup> ions, respectively.<sup>5-7</sup> According to the literature,<sup>8</sup> the AAO template is composed of amorphous aluminum hydroxide, oxy-hydroxide, and hydrated aluminum oxide. The existence of lattice oxygen and hydroxyl ions is consistent with the composition of AAO template. In contrast,  $\text{Zn}_{0.1}\text{t}_{12}$  and  $\text{Ni}_{1.0}\text{t}_{12}$  show O 1s BE value of about 532.1 eV, which can be attributed to the surface OH anions of LDH structure.<sup>9</sup>

Table S1 EDX<sup>a</sup> analysis of M/Al molar ratio of Zn<sub>0.1</sub>t<sub>y</sub> (y = 1, 6, 12, and 24 h) and Ni<sub>1.0</sub>t<sub>y</sub> (y = 0.5, 1, 6, 12, and 24 h).

Reaction time (h)	Zn/Al		Ni/Al	
	Outer surface	Cross section	Outer surface	Cross section
0.5			0.007	0.008
1	0.010	0.006	0.033	0.010
6	0.027	0.014	0.067	0.031
12	0.641	0.023	0.155	0.030
24	0.929	0.011	0.159	0.022

<sup>a</sup> Detect region of about 10 μm × 10 μm.

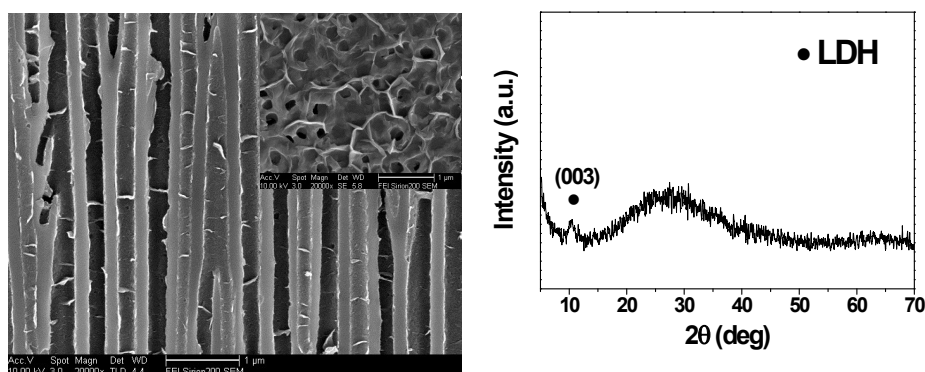


Fig. S4 SEM images and XRD pattern of Zn<sub>0.1</sub>t<sub>12</sub>(pH<sub>4.0</sub>) prepared at pH 4.0.

We prepared Zn<sub>0.1</sub>t<sub>12</sub>(pH<sub>4.0</sub>) in a 0.1 M Zn<sup>2+</sup> solution, which pH had been lowered close to the natural pH of 0.5 M Zn<sup>2+</sup> solution. The stronger acidic condition induces much fewer nucleation and poor crystallinity of ZnAl-LDH. In view of the fact that the pH decreases with the increase of Zn<sup>2+</sup> concentration in reaction solutions, it is comprehensible that less ZnAl-LDH plates could be observed on Zn<sub>1.0</sub>t<sub>12</sub>.

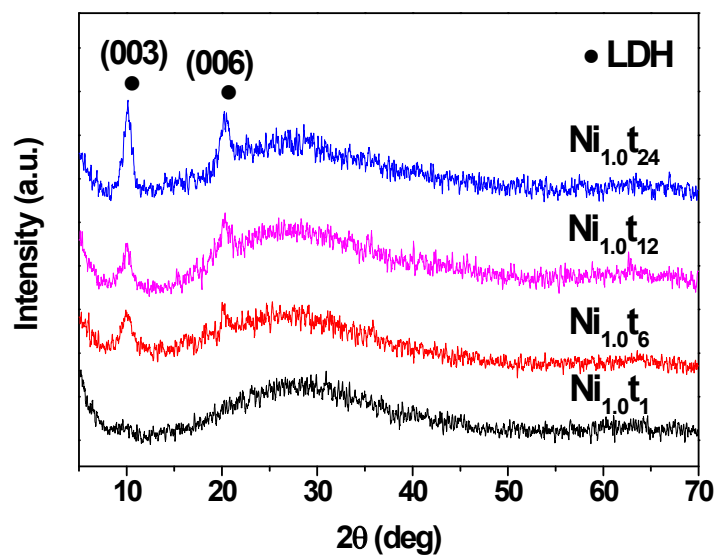


Fig. S5 XRD patterns of  $\text{Ni}_{1.0}\text{t}_y$  ( $y = 1, 6, 12,$  and  $24$  h) membranes.

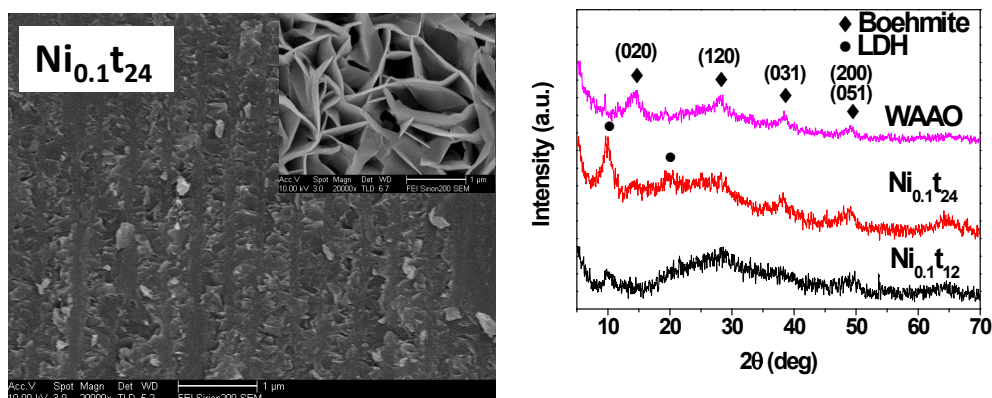


Fig. S6 SEM images of  $\text{Ni}_{0.1}\text{t}_{24}$ , and XRD patterns of WAAO,  $\text{Ni}_{0.1}\text{t}_{12}$ , and  $\text{Ni}_{0.1}\text{t}_{24}$ .

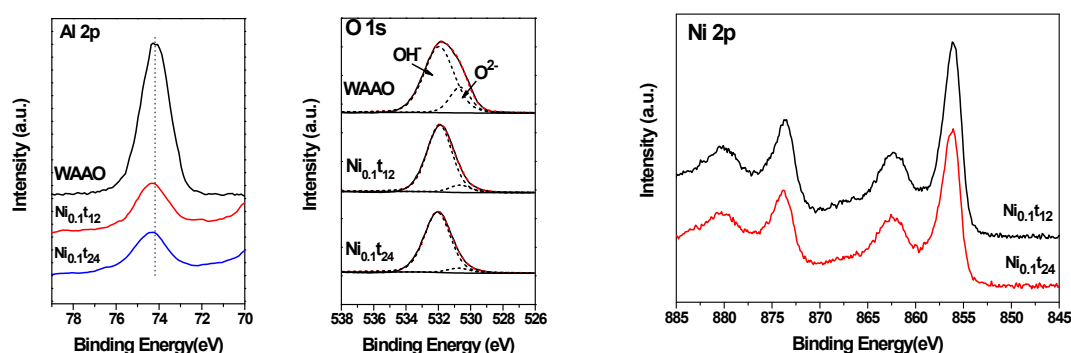


Fig. S7 XPS spectra of WAAO,  $\text{Ni}_{0.1}\text{t}_{12}$ , and  $\text{Ni}_{0.1}\text{t}_{24}$ .

The WAAO sample was prepared by substitution of deionized water for 0.1 M  $\text{Ni}^{2+}$  solution, and diffraction lines of pure boehmite are identified (Fig. S6). SEM images and XRD patterns in Fig. S6 show that plates on  $\text{Ni}_{0.1}\text{t}_{24}$  are larger and better-crystallized than those on  $\text{Ni}_{0.1}\text{t}_{12}$ . At the same time, both NiAl-LDH and boehmite exhibit the reinforcement of the characteristic reflections at 24 h. The XPS spectra of WAAO,  $\text{Ni}_{0.1}\text{t}_{12}$ , and  $\text{Ni}_{0.1}\text{t}_{24}$  are shown in Fig. S7. The O 1s peak of WAAO is composed of two peaks, which could be assigned to  $\text{O}^{2-}$  (530.7 eV) and  $\text{OH}^-$  (532.0 eV) of boehmite, respectively.<sup>10</sup> Unlike WAAO, the  $\text{O}^{2-}$  contents in  $\text{Ni}_{0.1}\text{t}_{12}$  and  $\text{Ni}_{0.1}\text{t}_{24}$  are reduced greatly because of the formation of NiAl-LDH, and no distinct difference of O 1s peak is observed between  $\text{Ni}_{0.1}\text{t}_{12}$  and  $\text{Ni}_{0.1}\text{t}_{24}$ . Both the XRD and XPS results do not prove the transition from boehmite to LDH.

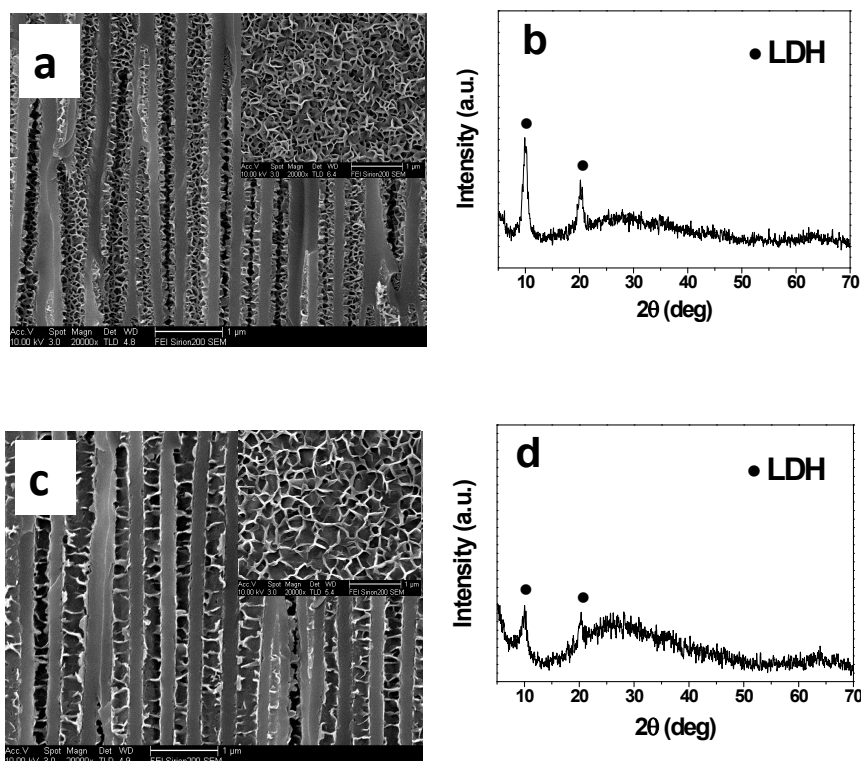


Fig. S8 SEM images and XRD patterns, (a, b)  $\text{Ni}_{1.0}\text{t}_{12}(\text{pH}_{4.4})$ , (c, d)  $\text{Ni}_{0.1}\text{t}_{12}(\text{pH}_{3.1})$ .

We prepared  $\text{Ni}_{1.0}\text{t}_{12}(\text{pH}_{4.4})$  and  $\text{Ni}_{0.1}\text{t}_{12}(\text{pH}_{3.1})$  in solutions with pH close to the natural pH of 0.1 M  $\text{Ni}^{2+}$  solution and 1.0 M  $\text{Ni}^{2+}$  solution, respectively. SEM images and XRD patterns in Fig. S8 show that uniform NiAl-LDH plates grow on the outer and inner surfaces without coexisting boehmite phase. As for  $\text{Ni}_{1.0}\text{t}_{12}(\text{pH}_{4.4})$ , the high concentration of 1.0 M  $\text{Ni}^{2+}$  prevents the growth of boehmite, and lead to successful fabrication of three-dimensional LDH/AAO membrane. The higher pH induces increases in crystallinity and size of NiAl-LDH, in comparison with  $\text{Ni}_{1.0}\text{t}_{12}$  prepared at natural pH  $\sim 3.1$  of 1.0 M  $\text{Ni}^{2+}$  solution. On the other hand, the acidification of 0.1 M  $\text{Ni}^{2+}$  solution slow down the formation of boehmite on  $\text{Ni}_{0.1}\text{t}_{12}(\text{pH}_{3.1})$ . Fig. S8(c) and (d) prove that only diffraction lines of LDH can be observed in XRD pattern of  $\text{Ni}_{0.1}\text{t}_{12}(\text{pH}_{3.1})$ . Benefiting from the lowered pH of 0.1 M  $\text{Ni}^{2+}$  solution, the pores of membranes are unblocked. The size and quantity of LDH plates are of evident difference between  $\text{Ni}_{1.0}\text{t}_{12}(\text{pH}_{4.4})$  and  $\text{Ni}_{0.1}\text{t}_{12}(\text{pH}_{3.1})$ .

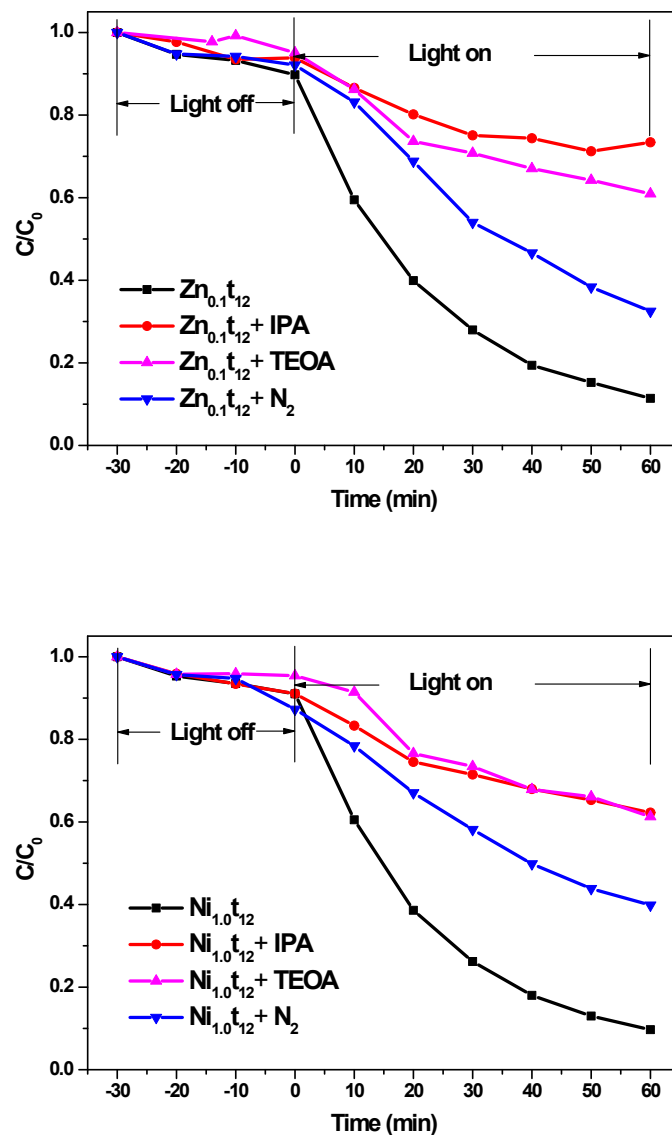


Fig. S9 Charge carrier trapping experiments over  $\text{Zn}_{0.1}\text{t}_{12}$  and  $\text{Ni}_{1.0}\text{t}_{12}$ .

Charge carrier trapping experiments have been studied using  $\text{N}_2$ , isopropanol (IPA), and triethanolamine (TEOA) as scavengers for  $\cdot\text{O}_2^-$ ,  $\cdot\text{OH}$ , and  $\text{h}^+$ , respectively, to elucidate the dominant reactive species involved in the degradation process. The results in Figure S9 indicate that the  $\cdot\text{OH}$  and  $\text{h}^+$  mainly govern the photocatalytic process, and  $\cdot\text{O}_2^-$  plays a minor role.<sup>11,12</sup>

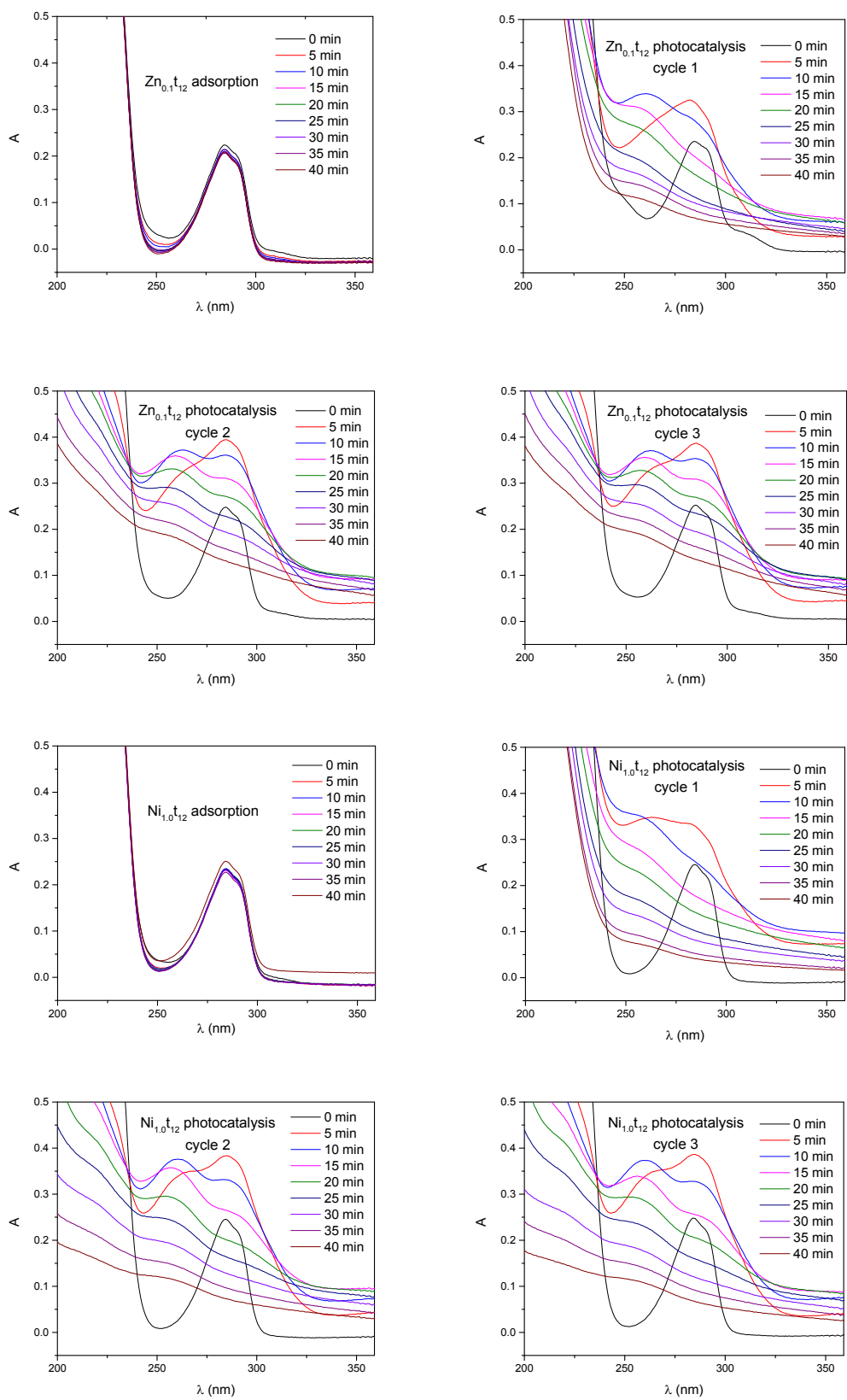


Fig. S10 Adsorption and three consecutive photocatalytic degradation cycles of 2,4-DCP on  $Zn_{0.1}t_{12}$  and  $Ni_{1.0}t_{12}$ .

The stability tests are performed when the colorless 2,4-dichlorophenol (2,4-DCP) solutions are used to rule out the possible dye sensitization effect. The adsorption of 2,4-DCP on  $Zn_{0.1}Ti_2$  and  $Ni_{1.0}Ti_2$  is very weak, and most 2,4-DCP can be photocatalytic degraded in 40 min indicating the high catalytic activity of catalysts. The catalytic activity tends to be stable with a slight reduction after the first cycle of photocatalytic degradation of 2,4-DCP. During the reaction, both the increase in the initial concentration of the contaminants (hyperchromic shift), and the small shift of the absorption band in the lower wavelength region may be caused by the possibility of formation of some intermediates.

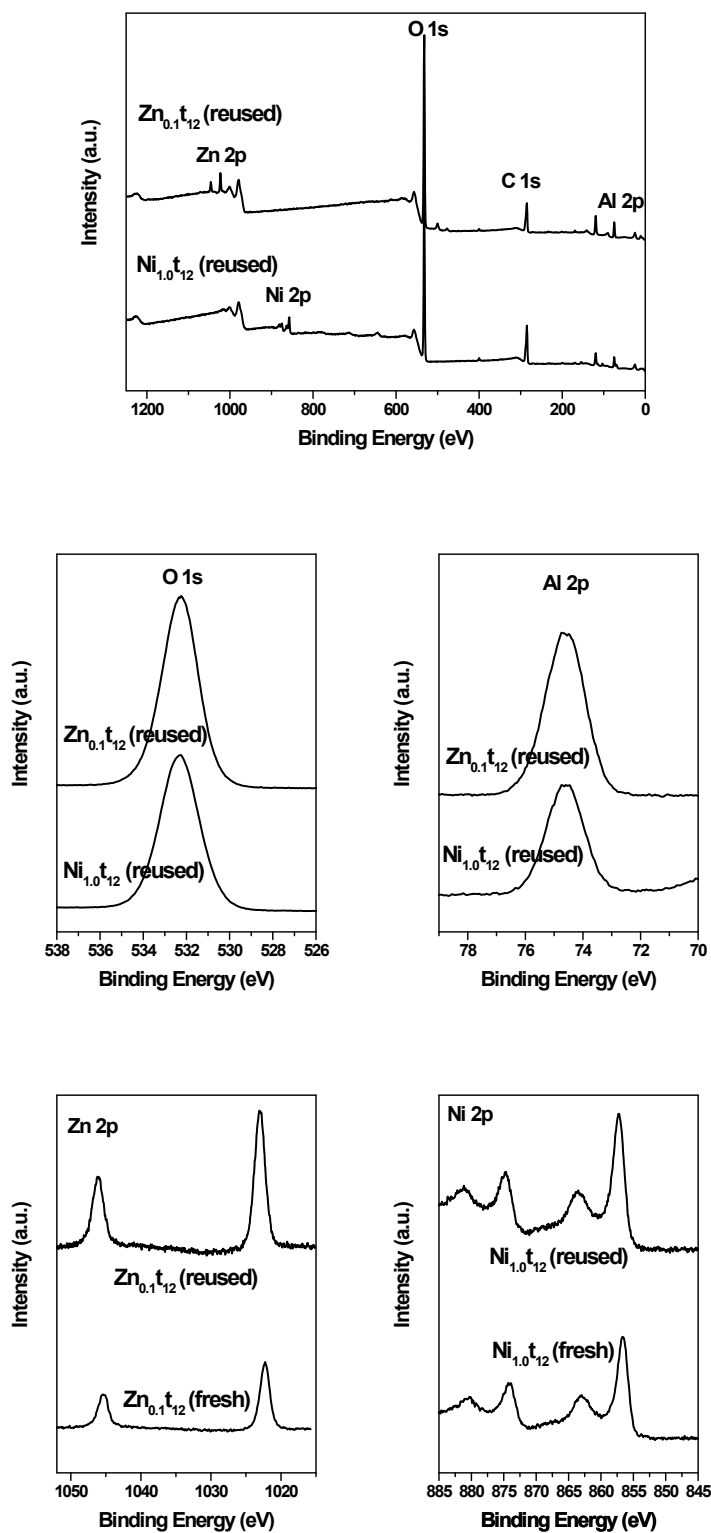


Fig. S11 XPS spectra of reused (after three cycles of photocatalytic test) and fresh Zn<sub>0.1</sub>t<sub>12</sub> and Ni<sub>1.0</sub>t<sub>24</sub>

Catalysts after three photocatalytic degradation cycles of 2,4-DCP are investigated by XPS. The XPS spectra in Figure S11 show that the O 1s binding energy (BE)

values are about 532 eV, and Al 2p BE values are approximately at 74.6 eV in  $Zn_{0.1}t_{12}$  and  $Ni_{1.0}t_{12}$ . These BE values are similar to those in Figure S3. The BE values of Zn  $2p_{3/2}$  and Ni  $2p_{3/2}$  of fresh and reused catalysts are approximately at 1022.4~1023 eV and 856.6~857.2 eV, respectively. The distinct difference between fresh catalyst and reused catalyst has not be observed.

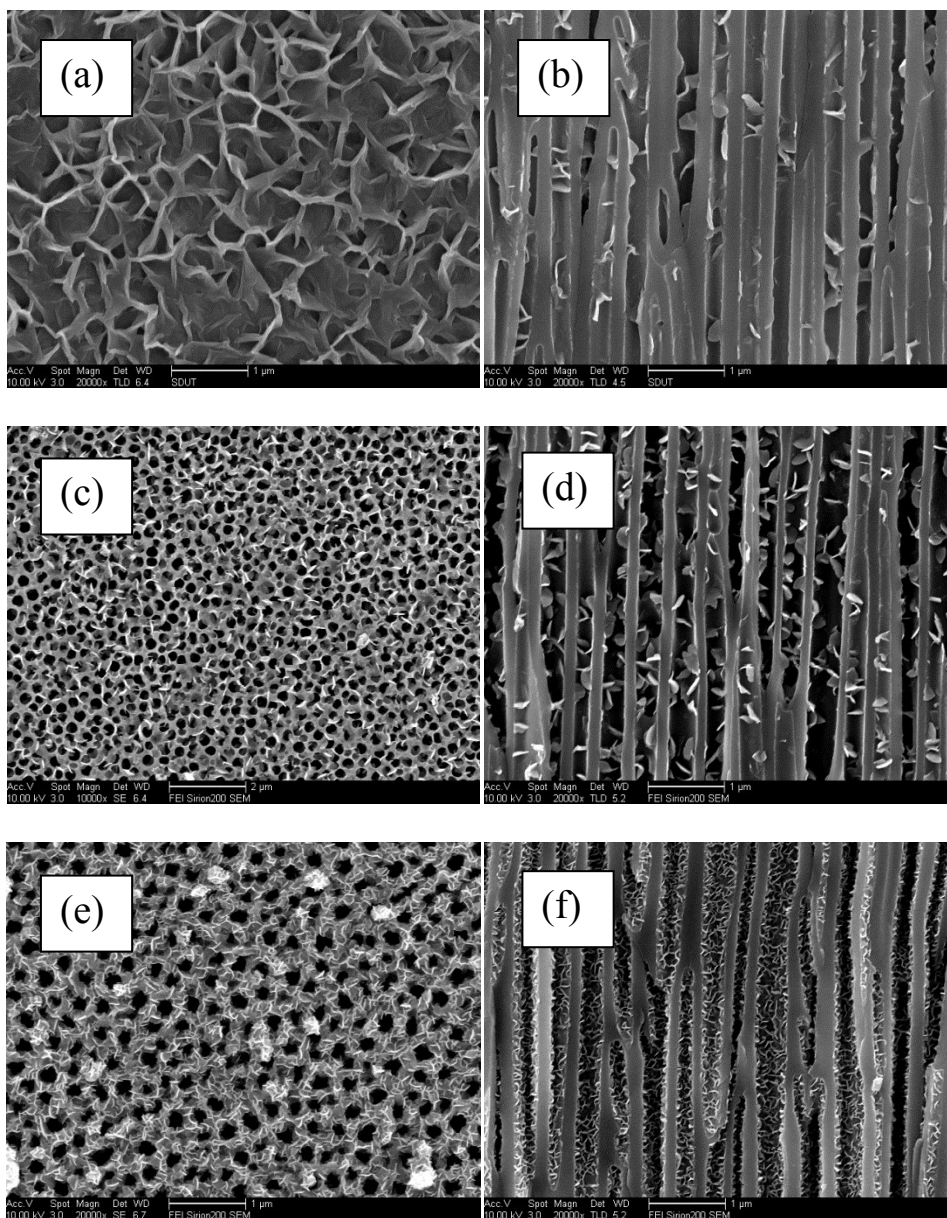


Fig. S12 SEM images, (a, b)  $\text{Co}_{1.0}\text{t}_{12}$ , (c, d)  $\text{Co}_{1.0}\text{t}_{24}$  (70 °C, in ethanol), (e, f)  $\text{Ni}_{1.0}\text{t}_{24}$  (70 °C, in ethanol).

## References

- 1 L. Xue, Y. Cheng, X. Sun, Z. Zhou, X. Xiao, Z. Hu and X. Liu, *Chem. Commun.*, 2014, **50**, 2301.
- 2 J. T. Klopogge, L. Hickey and R. L. Frost, *J. Solid State Chem.*, 2004, **177**, 4047.
- 3 K. Li, N. Kumada, Y. Yonesaki, T. Takeji, N. Kinomura, H. Wang and C. Wang, *Mater. Chem. Phys.*, 2010, **121**, 223.
- 4 E. Scavetta, B. Ballarin, C. Corticelli, I. Gualandi, D. Tonelli, V. Prevot, C. Forano and C. Mousty, *J. Power Sources*, 2012, **201**, 360.
- 5 Y. F. Gao, M. Nagai, Y. Masuda, F. Sato, W. S. Seo and K. Koumoto, *Langmuir*, 2006, **22**, 3521.
- 6 G. Morales-Mendoza, F. Tzompantzi, C. García-Mendoza, R. López, V. De la Luz, S.-W. Lee, T.-H. Kim, L. M. Torres-Martínez and R. Gómez, *Applied Clay Science*, 2015, **118**, 38.
- 7 H. Yan, J. Wang, Y. Zhang and W. Hu, *J. Alloys Compd.*, 2016, **678**, 171.
- 8 F. Le Coz, L. Arurault and L. Datas, *Mater. Charact.*, 2010, **61**, 283.
- 9 F. Li, L. Zhang, D. G. Evans and X. Duan, *Colloids and Surfaces A: Physicochemical and Engineering Aspects*, 2004, **244**, 169.
- 10 J. T. Klopogge, L. V. Duong, B. J. Wood and R. L. Frost, *J. Colloid Interface Sci.*, 2006, **296**, 572.
- 11 K. Yang, J. Li, Y. Peng and J. Lin, *Phys.Chem.Chem.Phys.*, 2017, **19**, 251.
- 12 H. Li, Q. Deng, J. Liu, W. Hou, N. Du, R. Zhang and X. Tao, *Catal. Sci. Technol.*, 2014, **4**, 1028.